Snow grain-size measurements in Antarctica

Michel GAY,[1,2] Michel FILY,[1] Christophe GENTHON,[1] Massimo FREZZOTTI,[3] Hans OERTER,[4] Jan-Gunnar WINTHER[5]

[1]*Laboratoire de Glaciologie et Géophysique de l'Environnement du CNRS, 54 rue Molière, BP 96, 38402 Saint-Martin-d'Hères, France*
E-mail: michel.gay@cemagref.fr
[2]*Cemagref, Domaine universitaire, 2 rue de la Papeterie, BP 76, 38402 Saint-Martin-d'Hères Cedex, France*
[3]*ENEA, Centro Ricerche Casaccia, P.O. Box 2400, I-00100 Rome, Italy*
[4]*Alfred Wegener Institute for Polar and Marine Research, P.O. Box 120161, D-27515 Bremerhaven, Germany*
[5]*Norwegian Polar Institute, Polar Environmental Centre, N-9296 Tromsø, Norway*

ABSTRACT. Grain-size is an important but not well-known characteristic of snow at the surface of Antarctica. In the past, grain-size has been reported using various methods, the reliability, reproducibility and intercomparability of which is not warranted. In this paper, we present and recommend, depending on available logistical support, three techniques of snow-grain sampling and/or imaging in the field as well as an original digital image-processing method, which we have proved provides reproducible and intercomparable measures of a snow grain-size parameter, the mean convex radius. Results from more than 500 samples and 3000 images of snow grains are presented, which yield a still spatially limited yet unprecedentedly wide picture of near-surface snow grain-size distribution from fieldwork in Antarctica. In particular, except at sites affected by a very particular meteorology, surface grains in the interior of the ice sheet are uniformly small (0.1–0.2 mm). The climate-related increase of grain-size with depth through metamorphism is, as expected, not spatially uniform. Our Antarctic snow grain-size database will continue to grow as field investigations bring new samples, images and measures of snow grain.

INTRODUCTION

The knowledge of snow surface characteristics of ice sheets is important for many reasons. The snowpack is the interface between the atmosphere and the underlying ice, controlling the exchange of energy and mass (Brun and others, 1989, 1992). The albedo of snow depends on the snow effective grain-size and the surface characteristics (Grenfell and others, 1994; Marshall and Oglesby, 1994; Winther, 1994; Fily and others, 1998). The snow is the initial stage of the densification and trapping of air in the firn and the ice (Alley and Bentley, 1988; Arnaud and others, 1998), and finally the snow physical characteristics control the remote-sensing measurements (Alley, 1987; Bindschadler, 1998; Fily and others, 1998, 1999; Genthon and others, 2001).

Most physical properties of snow and ice cover are clearly defined and measurable except for the grain geometry which can be difficult to characterize (Colbeck and others, 1990; Colbeck 1991). A simple method suitable for field measurements of grain-size is to place a sample of snow grains on a ruled plate. The average size is then estimated by comparing the mean size of the grains with the marks on the plate. The definition of size is not unique for three-dimensional non-isotropic objects. One common definition of grain-size is the greatest extension of the grains (Colbeck and others, 1990) measured in millimeters or classified from "very fine" ($<$0.2 mm) to "very coarse" (2.0–5.0 mm). For the purpose of reflectance modelling, Grenfell and others (1994) used the same technique to measure the smallest, rather than the greatest, extension, which is generally closer to the diameter of an equivalent sphere with the same surface/volume ratio. An approximate distribution of grain-sizes may also be obtained by snow sieving or by automated image-processing techniques. Many other definitions of grain-size can be found (Alley, 1987) and this must be taken into account when comparing measurements reported by different authors.

Our goal in this paper is to propose an objective method to determine one well-defined snow grain-size parameter. Because the method is objective and reproducible, measurements made at different places and times by different operators are quantitatively comparable. The method is based on the analysis of digital images of snow grains. First, in a technical section, we describe the image-acquisition techniques and the numerical algorithm to determine grain-size from the images. Then, in a results section, data obtained from a large number of samples and images collected in different places in Antarctica are presented and discussed (Fig. 1). The samples were collected as part of national or international Antarctic scientific traverses (e.g. Winther and others, 1997). The spatial and depth coverage of the current archive is still very limited. It is expected to progressively develop into a comprehensive dataset of snow images and grain-sizes as new exploratory traverses (e.g. as part of International Trans-Antarctic Scientific Expeditions (ITASE); Mayewski and Goodwin, 1999) bring more high-quality data.

IMAGE-ACQUISITION TECHNIQUES

Slices of high-density firn can be cut, and thick sections have been produced with microtome before an image of the sur-

https://doi.org/10.3189/172756502781831016 Published online by Cambridge University Press

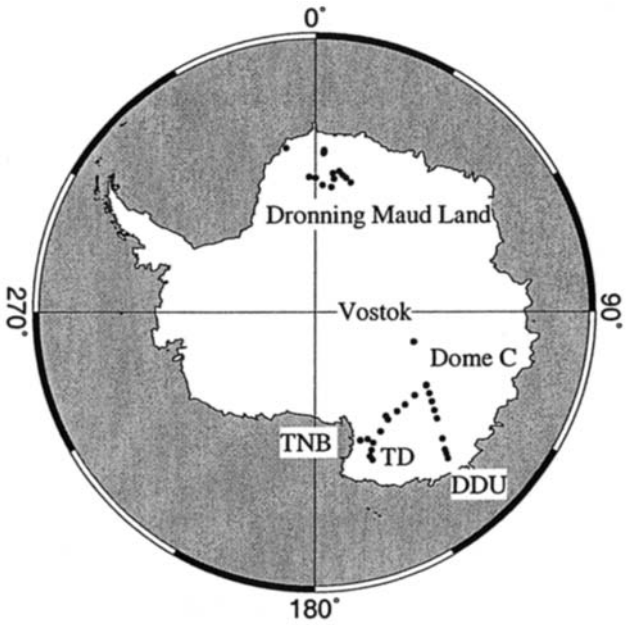

Fig. 1. Antarctic map showing location of sampling sites. TNB, Terra Nova Bay; DDU, Dumont d'Urville; TD, Talos Dome.

face is taken (Arnaud and others, 1998). The process cannot be applied to lower-density snow in the upper meters of the snowpack, unless cohesion is increased by impregnation before slicing (Alley, 1980; Good, 1989). This is technically too difficult and too labour-intensive to be implemented in situ on a regular basis. We have tested three lighter techniques to acquire digital images of snow grains.

Technique 1: Snow samples are collected in small flasks filled with isooctane (trimethyl 2-2-4-pentane) to prevent metamorphism after collection (Brun and Pahaut, 1991). The samples are then kept at temperatures well below freezing and transported to the Laboratoire de Glaciologie et Géophysique de l'Environnement (LGGE) where digital images are taken in a cold laboratory. For this, a binocular microscope is used with a mounted digital camera linked to a computer. After drying on filter paper, snow grains and clusters are separated (using a toothpick-like tool) on a glass window and illuminated from below (transmitted light). The magnifying factor depends on the mean grain-size. It is chosen to be between 2 and 3, so that three to four grains or clusters are captured on each image (Fig. 2a). Technique 1 (Lesaffre and others, 1998) was used at all sites for which results are presented in section 3. Additionally, other methods were tested at some of the sampling sites.

Technique 2: Classic (film) macrophotographies of snow grains are taken in the field and then digitized at LGGE (Fig. 2b). A 50 mm macro-lens and an additional ring set the magnifying factor to 2. In this case, the grains are dispersed on a dark plate and the illumination is diffuse from above (reflected light). As the film definition is very good, a second enlargement can be obtained when digitizing the slides. Technique 2 was used along a Terra Nova Bay–Dome Concordia (Dome C) traverse (Fig. 1).

Technique 3: Digital images were acquired in the field when adequate facilities were available. This was done at Dome C (Fig. 1) where a digital camera was available in a cold laboratory close to the sampling site. Because of the material resources needed, technique 3 may be used at a fixed point but generally not on traverses.

About 50 different grains (i.e. about 15 images, each showing 3–4 grains) of each snow sample were analyzed to obtain a statistically significant measure of the mean size. Dispersal and separation of grains for each image, a rather

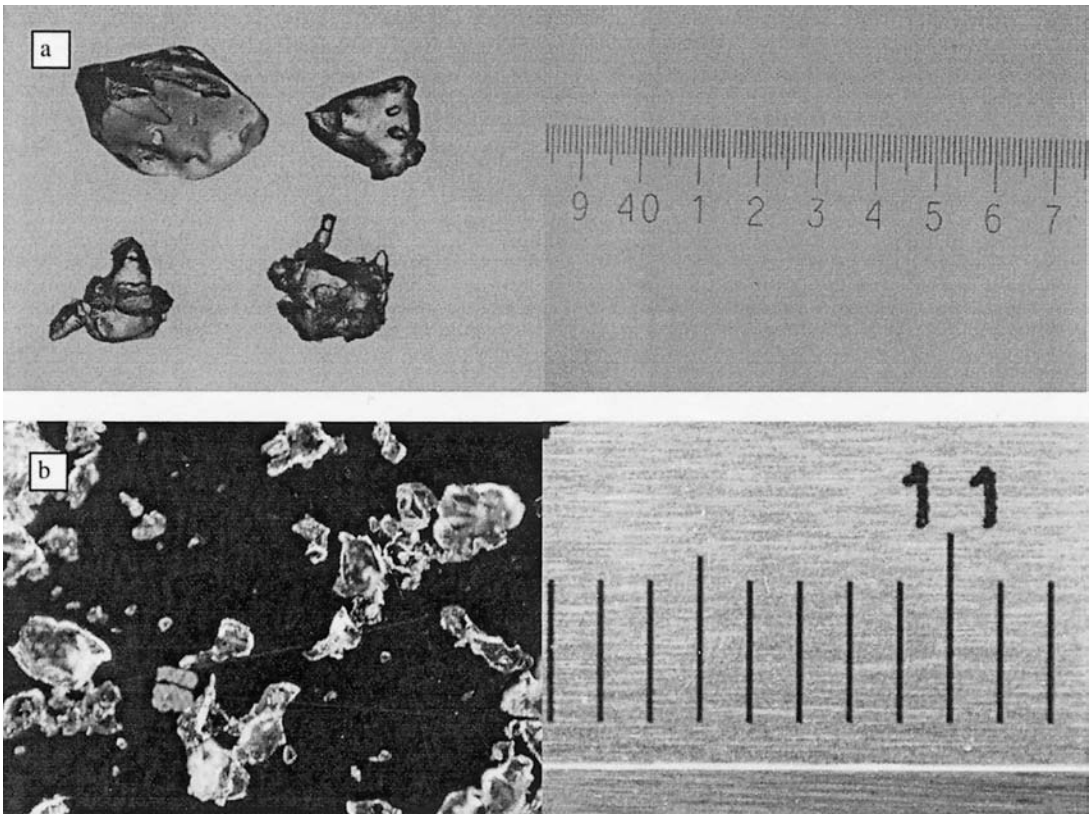

Fig. 2. (a) Digital image of snow grains collected in the field and transported in isooctane (technique 1) with scale in 1/10 mm. (b) Photograph of snow grains acquired in situ (technique 3) at the same site (itb8 at 1.5 m depth) along the Terra Nova Bay–Dome C traverse with scale in mm.

https://doi.org/10.3189/172756502781831016 Published online by Cambridge University Press

delicate and time-consuming operation, may be hard to accomplish in the field. On the other hand, taking photographs directly in the field (techniques 2 and 3) may be safer than sampling in isooctane flasks for imagery back in the laboratory (technique 1). Indeed, over the past few years, a number of snow samples have been lost due to insufficiently cold conditions during transport. Our results prove that all of the three above techniques yield good results and may be recommended, depending on the logistical and technical support available in the field and for the transport phase.

Digital image processing

Perfect separation of snow grains for imagery is generally difficult and barely fully realized. Clustering of snow grains is a major problem, which prevents the use of stereologic quantities based on the area or the lengths of the objects to determine grain-sizes. To avoid biases associated with grain clustering, a size parameter is defined only from the contour of the snow grains or clusters: it is the mean radius of all the convex parts of the ice/air boundaries, or the mean convex radius. This parameter was found to be representative of the grain-size for metamorphism (Lesaffre and others, 1998). For example, it is the size parameter, along with dendricity and sphericity, used in the snow-metamorphism model Crocus (Brun and others, 1992). The mean convex radius was also found to be the best grain-size parameter for modelling of snow reflectance in the near-wave infrared spectral domain (Fily and others, 1997, 1999; Sergent and others, 1998).

For mean convex radius measurement, the contour of the object needs to be digitally identified from an original grey-scale image. This is done by transforming the grey image into a binary (black and white) image, a process called image segmentation.

Image segmentation

For each pixel $P(x, y)$ of an image, the local gradient $G(x, y)$ is obtained from the surrounding pixels using a Sobel operator over a 3×3 region:

$$G(x, y) = (G_x^2 + G_y^2)^{0.5}$$

with

$$G_x = (z_3 + 2z_6 + z_9) - (z_1 + 2z_4 + z_7)$$
$$G_y = (z_7 + 2z_8 + z_9) - (z_1 + 2z_2 + z_3)\,,$$

where the z's are the grey levels of the pixels, z_5 corresponding to pixel $P(x, y)$ (Table 1).

Once the procedure is completed for all possible pixels, the result is a gradient image of the same size as the original image (Fig. 3a). The lines of highest gradients, above a minimum threshold (Fig. 3b), define discrete contours. Each object is then defined as the set of connected pixels whose gradient value is less than this minimum threshold. The image "background" is given the value 1, and all the objects (the grains) the value 0. The result is a binary image with each object being a grain or a cluster of grains (Fig. 3c).

Table 1. Grey-level indices used for the Sobel operator

z_1	z_2	z_3
z_4	z_5	z_6
z_7	z_8	z_9

Mean convex radius

The mean convex radius may simply be computed as the mean radius of curvature of the curves locally fitting the discrete contour where it is convex (Lesaffre and others, 1998). The accuracy of this method depends on the number N of contour pixels used to fit the discrete contour, and errors can be as high as 30%. In order to reduce the error, N must be optimized depending on the size of the grains on the digital image. Therefore, as N is kept constant, it is necessary to adapt the magnifying factor to the grain-size, which is not possible when there is a large range of grain-sizes on the same image. To overcome this problem, we use an alternate method based on the skeletization of each object (grain) on an image. This method is more robust and can provide various size parameters depending on the final application.

The weighted skeleton is a reduced but complete representation of an object. The construction of a skeleton (Sanniti di Baja and Thiel, 1996) requires determination of the distance between each object pixel and the object boundary. Consider a digital binary image, consisting of object and non-object pixels (Fig. 3c). We use a distance transformation which is an operation that converts this binary image to a grey-level image, where each object pixel has a value corresponding to the distance to the nearest contour pixel (Fig. 3d). The new image is called a distance map and can be interpreted as the result of a propagation process: a wave front originating from the object contour propagates at uniform speed towards the inside. This is described in detail in Sannitti di Baja and Thiel (1996). In particular, we use the chamfer distance transformation on a 5×5 pixel neighborhood (Borgefors, 1986; Thiel, 1994; Sanniti di Baja and Thiel, 1996) as a practical proxy for Euclidean distance. The difference with actual Euclidean distance is, in this case, then $< 2\%$.

From the distance map the skeleton is found. If we consider the distance map as a topographic map, with the highest pixels associated to the largest distances, the skeleton can be simply defined as the ridges of this topographic surface. For a two-dimensional digital image it is defined as the locus of centers of maximal disks contained in the object (Fig. 3e). A skeleton is composed of branches with nodal points at their intersections and end-points at their extremities.

A maximal disk, and therefore a radius, contained in the object can be associated to each pixel of the discrete skeleton (Chassery and Montanvert, 1991). In particular, one radius is associated to each end-point of the skeleton which is representative of the convexity of the contour close to it (Fig. 3e). The mean convex radius is the average of all these radii. The radii associated to nodal points of the skeleton are more representative of the volume of the grains, or clusters of grains. The weighted skeleton could also provide information on the shape of the grain (Chassery and Montanvert, 1991), but this is beyond the scope of this paper.

RESULTS

Comparison of sampling and image-analysis techniques

Images of more than 500 snow samples were collected for different locations and depths in Antarctica, thanks to the activity of French, German, Italian and Norwegian field parties in recent years (Table 2; Fig. 1). Sampling technique 1 (isooctane flasks) was systematically used at all sites and

https://doi.org/10.3189/172756502781831016 Published online by Cambridge University Press

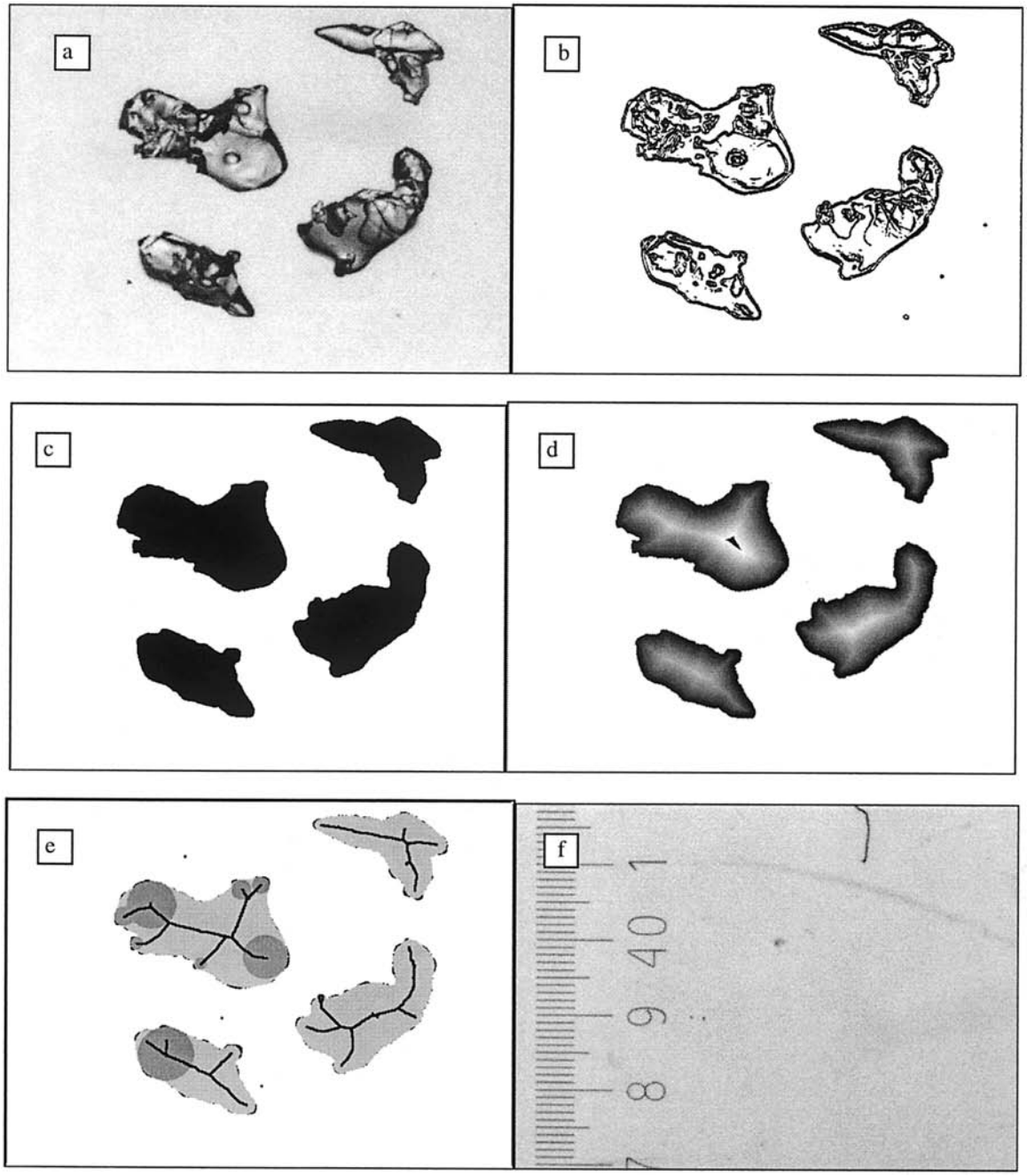

Fig. 3. (a) Original image of a few snow grains; (b) gradient image; (c) binary image; (d) distance map; (e) skeleton and examples of maximal disks contained in the snow grains; (f) scale in 1/10 mm.

along all traverses. Techniques 2 or 3 (imagery on the field) were also used at Dome C and along the Terra Nova Bay–Dome C traverse. All images (about 3000 altogether) were processed with the same image-analysis method for grain-size determination, as described above. The equivalence of the different sampling techniques can thus be assessed.

All the results are given in Figures 4–6. To allow a simple visual comparison of the grain-sizes, the same scale, but not the same range, is used for all the sites. The error bars represent the standard deviation of all the mean convex radii obtained for one sample.

At Dome C (Fig. 4) the sizes obtained from isooctane samples (technique 1) and from digital images (technique 3) acquired 2 years later are very similar. This demonstrates (1) that snow metamorphism in cold isooctane during transportation and storage in good conditions is negligible, and (2) that the same results are obtained when different techniques are applied by different operators at different times. This is further confirmed by Figure 5, which compares grain-sizes along a Terra Nova Bay–Dome C traverse as obtained from photographs taken in the field (technique 2) and from snow samples brought back to LGGE (technique 1). Photographs visibly showing massive clustering and insufficient separation of grains were discarded. In most cases, results from both techniques are very similar. Large differences may be found in some places because the samples were not taken in exactly the same layer and because the grains were too clustered.

From the same weighted skeleton, different size parameters can be computed. The radii computed from end-points and nodal points are compared for many sites (Fig. 6). Examples of digital images of snow grains are given for the two sites aw2 and aw6 in Figure 7. When the grains are well separated and easily identified (Fig. 7a; aw6 at 0.4 m) the two size parameters are similar (~0.15 mm). When the grains are clustered (Fig. 7b; aw2 at 0.2 m), the nodal radius (~0.5 mm) is larger than the end-point radius (0.1 mm) because it is more sensitive to the volume of the object than

https://doi.org/10.3189/172756502781831016 Published online by Cambridge University Press

Table 2. Sampling locations and dates

Sample	*Lat., long.*	*Altitude* m	*Date*	*Site*
aw1	71.45° S, 9.94° W	600	13 Feb. 1997	DML
aw2	74.86° S, 2.55° W	2830	13 Jan. 1997	DML
aw3	75.00° S, 0.01° E	2890	16 Jan. 1997	DML
aw4	75.75° S, 3.28° E	2970	22 Jan. 1997	DML
aw5	75.93° S, 7.21° E	3150	28 Jan. 1997	DML
aw6	74.40° S, 7.22° E	3180	24 Jan. 1997	DML
aw7	75.00° S, 8.01° E	3245	26 Jan. 1997	DML
ita1	74.82° S, 160.66° E	1270	8 Nov. 1996	TNB-Talos
ita2	74.64° S, 157.50° E	1780	9 Nov. 1996	GPS2
ita3	74.03° S, 155.96° E	2060	10 Nov. 1996	3IDPT
ita4	73.37° S, 157.67° E	2205	11 Nov. 1996	PNI
ita5	72.80° S, 159.10° E	2305	23 Nov. 1996	Talos Dome
ita6	72.37° S, 158.75° E	2215	25 Nov. 1996	ST556
itb1	74.84° S, 160.82° E	1200	20 Nov. 1998	GPS 1
itb2	74.64° S, 157.50° E	1780	27 Nov. 1998	GPS2
itb3	74.03° S, 155.96° E	1925	1 Dec. 1998	3IDPT
itb4	74.80° S, 151.27° E	2310	6 Dec. 1998	M2
itb5	75.55° S, 145.79° E	2460	11 Dec. 1998	MDP
itb6	75.53° S, 145.92° E	2450	14 Dec. 1998	MDPA
itb7	75.62° S, 140.63° E	2610	20 Dec. 1998	D2
itb8	75.60° S, 135.83° E	2790	26 Dec. 1998	D4
itb9	75.45° S, 129.81° E	3025	31 Dec. 1998	D6
np1	71.90° S, 3.08° E	1455	31 Dec. 1996	DML
np2	72.13° S, 3.18° E	2040	4 Jan. 1997	DML
np3	72.25° S, 2.88° E	2300	5 Feb. 1997	DML
np4	74.05° S, 9.50° E	3280	31 Jan. 1997	DML
np5	74.35° S, 9.05° E	3270	30 Jan. 1997	DML
np6	74.65° S, 12.78° E	3420	29 Jan. 1997	DML
np7	75.00° S, 15.00° E	3470	25–28 Jan. 1997	DML
ta1	68.06° S, 137.72° E	2045	22 Nov. 1995	DDU-DC
ta2	68.55° S, 137.07° E	2320	22 Nov. 1995	DDU-DC
ta3	68.97° S, 136.47° E	2360	23 Nov. 1995	DDU-DC
ta4	70.03° S, 134.82° E	2495	25 Nov. 1995	DDU-DC
ta5	71.99° S, 131.18° E	2990	27 Nov. 1995	DDU-DC
ta6	72.77° S, 129.46° E	3125	28 Nov. 1995	DDU-DC
ta7	73.59° S, 127.48° E	3140	29 Nov. 1995	DDU-DC
ta8	74.36° S, 125.46° E	3185	30 Nov. 1995	DDU-DC
ta9	75.10° S, 123.00° E	3230	Dec. 1995	20 km around DC
DC	75.16° S, 123.23° E	3230	1997 and 2000	Dome C: 5 m profile
Vost	78.47° S, 106.80° E	3480	Dec. 1997	Vostok: 2 m profile

Notes: aw: Alfred Wegener Institute, Germany. ita and itb: samples from ENEA, Italy. np: samples from Norwegian Polar Institute. ta, DC and Vost: samples from LGGE/IFRTP, France. Elevations are from the RADARSAT Antarctic Mapping Project digital elevation model 400 m ellipsoid WGS84 geoid OSU91 "Data provided by the EOS Distributed Active Archive Center (DAAC) at the National Snow and Ice Data Center, University of Colorado, Boulder, CO". DML: Dronning Maud Land. TNB: Terra Nova Bay. DDU-DC: Dumont d'Urville–Dome C.

to the shape of its contour. As clustering of snow grains is difficult to avoid, we prefer to use the mean convex radius as defined from the skeleton end-points. This also emphasizes the importance of the definition of the size parameter when different samples are compared.

Spatial and depth variations of Antarctic snow grain-size

The results obtained from the 42 sites in Antarctica tend to show that near the surface (0–0.5 m) the mean convex radius is surprisingly spatially homogeneous, of the order of 0.1–0.2 mm almost everywhere. They may be classified as very fine to fine grain (<0.2 to 0.5 mm) according to Colbeck and others (1990). Comparison with other in situ data reported in the literature is difficult because the size was determined visually and therefore it does not represent the same parameter.

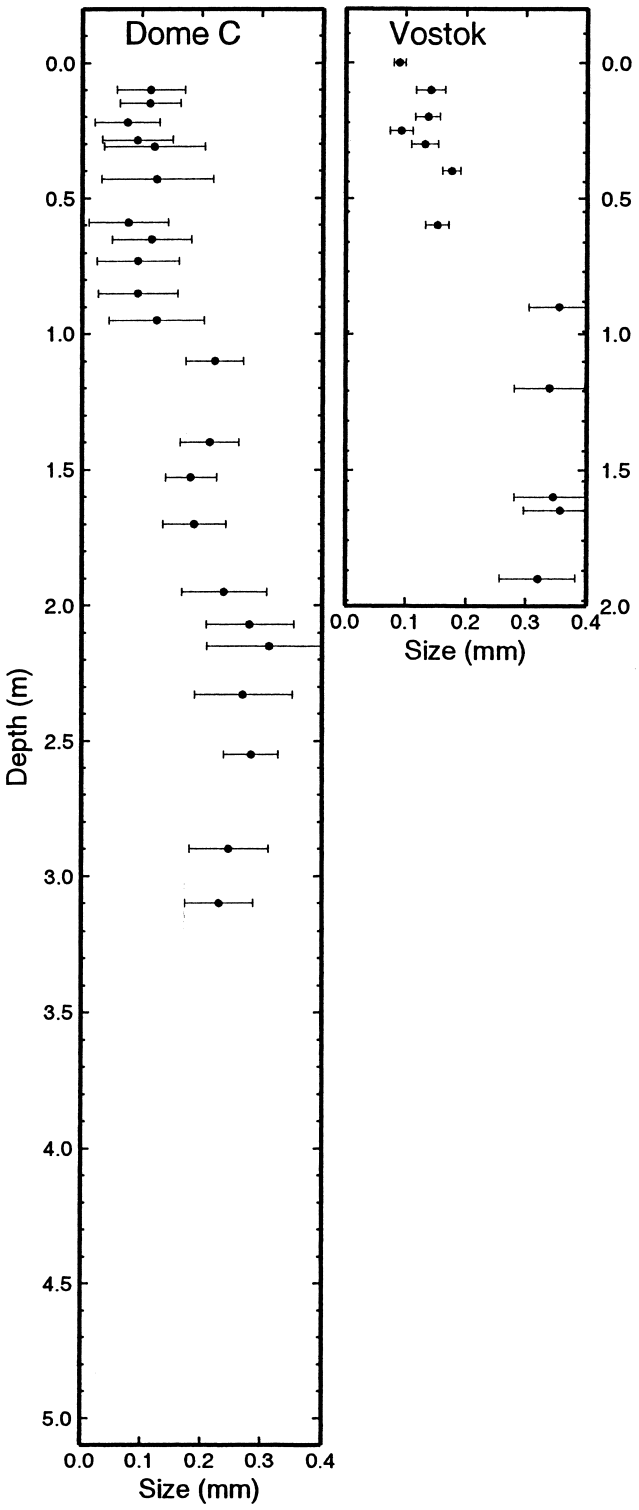

Fig. 4. Mean convex radius of snow grains vs depth at Dome C and Vostok. The error bars represent one standard deviation of all the measurements obtained for one sample. The dots (●) are from digital images of snow samples collected in the field in 1997 and transported to Grenoble in cold isooctane (technique 1). The squares (□) are from digital images acquired at Dome C in 2000 (technique 3).

The largest variability is found along the Terra Nova Bay–Dome C traverse (Figs 5 and 6). The sizes obtained from samples acquired at a 2 year interval are very similar for 31DPT (samples ita3 and itb3) and different for GPS2 (samples ita2 and itb2). GPS2 is a site with erosional forms up to 15 cm and seasonal wind crust, whereas 31DPT site presents depositional forms about 10 cm and has more homogeneous snow stratigraphy than GPS2. Larger grain-sizes are

https://doi.org/10.3189/172756502781831016 Published online by Cambridge University Press

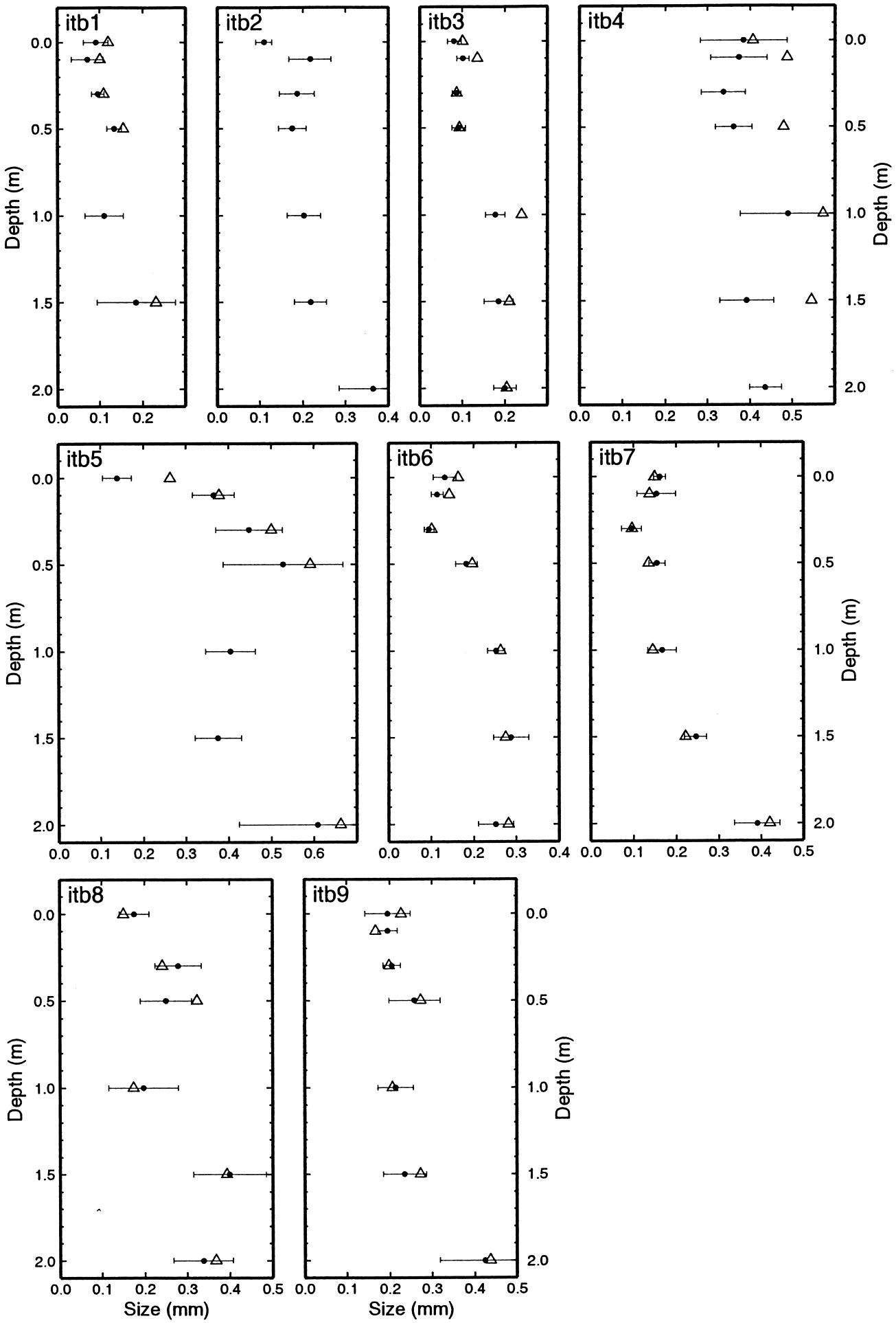

Fig. 5. Mean convex radius of snow grains vs depth along the Terra Nova Bay–Dome C traverse (Table 2; Fig. 1). The dots (●) are from digital images of snow samples collected in the field in 1997 and transported to Grenoble in cold isooctane (technique 1). The triangles (△) are from classical photos acquired in situ (technique 2).

https://doi.org/10.3189/172756502781831016 Published online by Cambridge University Press

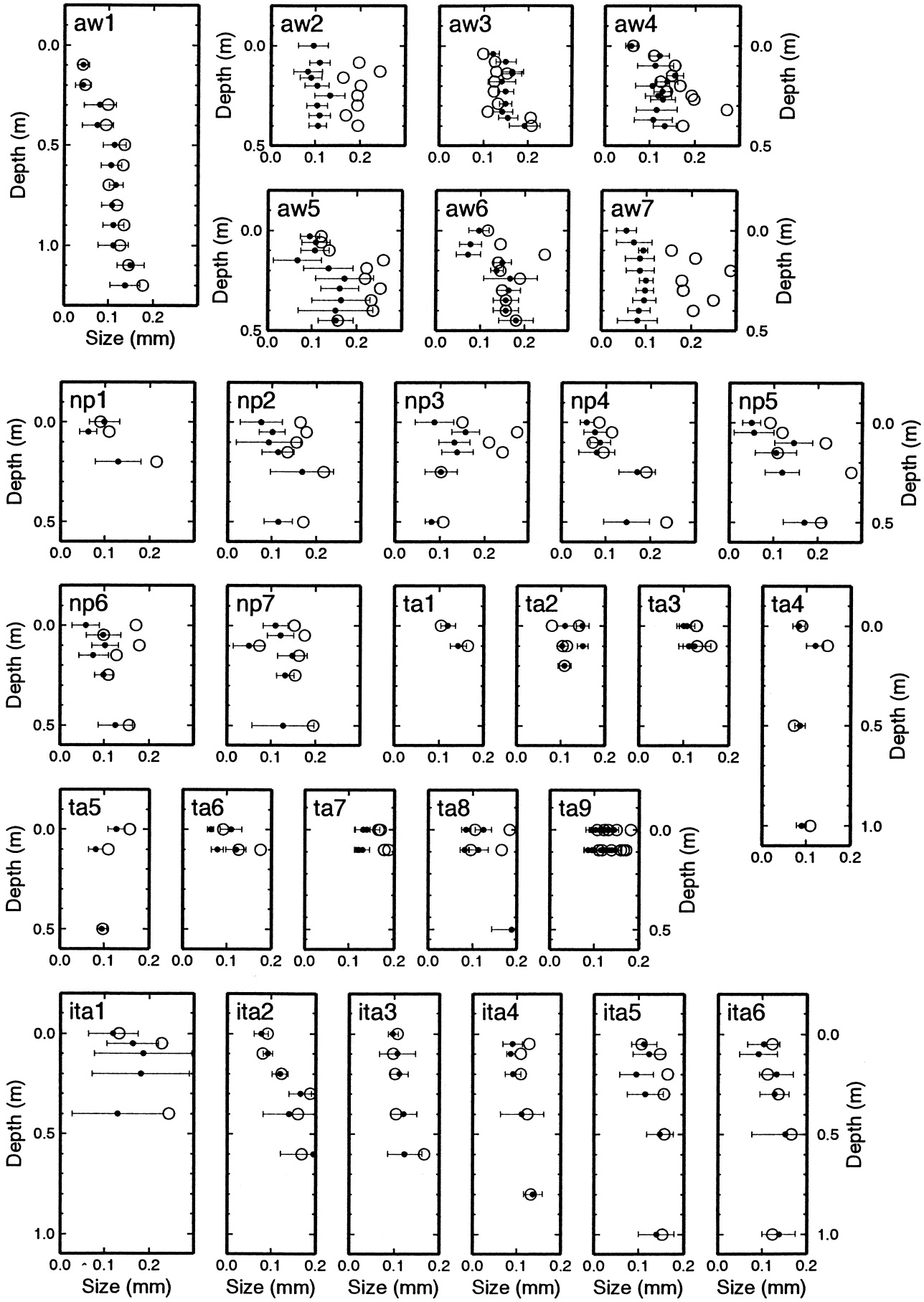

Fig. 6. Mean convex radius of snow grains vs depth along several traverses (Table 2; Fig. 1). Technique 1 is used for all the samples. The dots (●) are for radii corresponding to the end-points of the skeleton, and circles (○) are for nodal points.

found at M2 (itb4) and MDP (itb5) sites even at the surface. This is in agreement with older traverse data (Stuart and Heine, 1961) and could explain the peculiar microwave signature observed there (Surdyk and Fily, 1993). These sites are characterized by wind crust, consisting of a single snow-grain layer cemented by thin (0.1–2 mm) films of sublimated ice. Under strongly developed wind crust the depth-hoar layer clearly indicates prolonged sublimation due to a hiatus

https://doi.org/10.3189/172756502781831016 Published online by Cambridge University Press

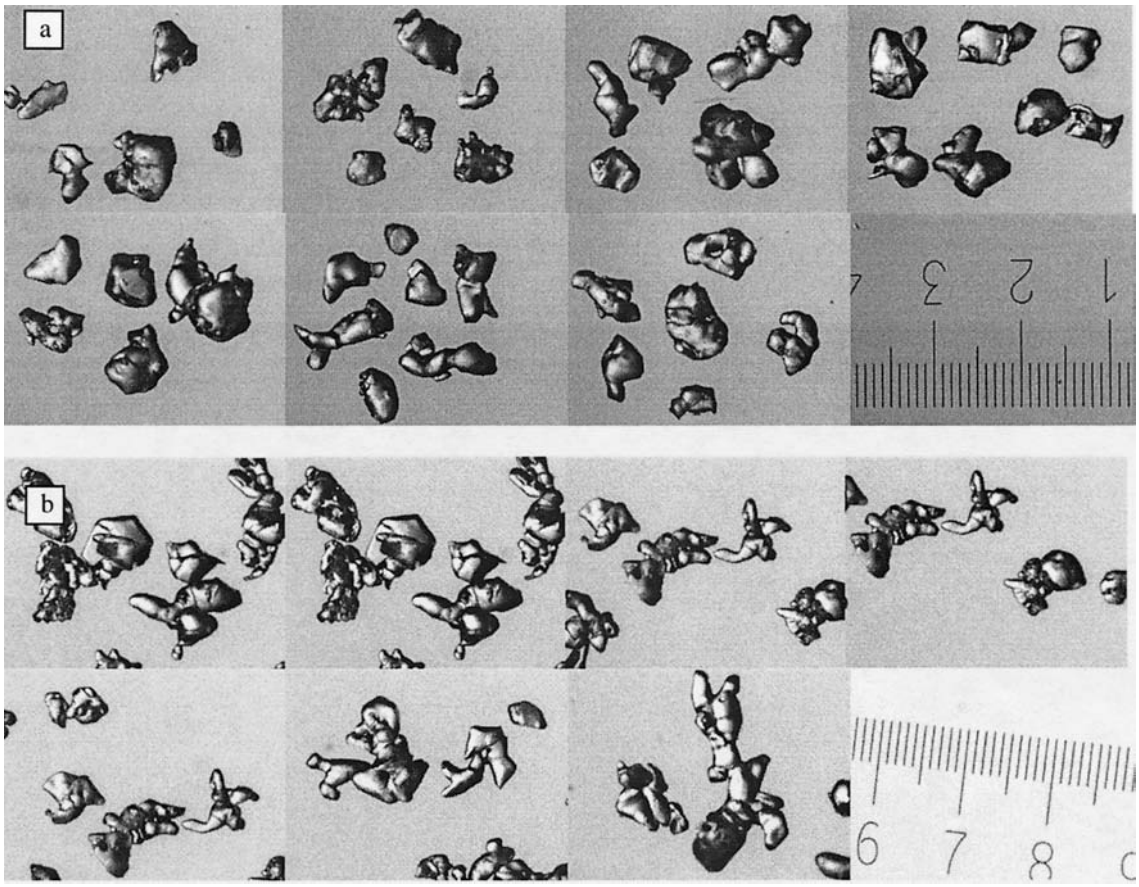

Fig. 7. Digital images (technique 1) of snow grains from the Dronning Maud Land area (Table 2; Fig. 1) with the corresponding scale in 1/10 mm: (a) site aw6 at 0.4 m depth; (b) site aw2 at 0.2 m depth.

in accumulation and therefore a long, multi-annual, steep temperature-gradient metamorphism (Gow, 1965). Either the large grain or the wind crust (Wiesmann and others, 2000) could explain the peculiar microwave signature observed (Surdyk and Fily, 1993). Sites MDP (itb5) and MDPA (itb6) are only at a distance of 5 km, and show quite different grain-size profiles, both for mean values and for variability. MDPA site shows sastrugi up to 20 cm high but no permanent wind crust. The large difference in grain-size between the two sites is due to the different snow-redistribution process at local scale. Frezzotti and others (2002) point out that along the Terra Nova–Dome C traverse, wind crusts are present in a wide area of the plateau, and are strictly correlated with snow-redistribution process due to downwind slope $>0.25^{\circ}$ (0.4% or 4 m km^{-1}).

At Vostok and Dome C, more variations in grain-size occur below 1 m, and a significant difference is found between the two sites. At Vostok, there is a sharp increase in grain-size between 0.6 and 0.8 m depth. The evolution of size is smoother at Dome C. The size is almost identical between 2 and 5 m as observed in situ.

All sites where the variations of size with depth are significantly sampled show a broad increase with depth. This is expected, as metamorphism tends to favor the growth of the larger grains with time, at the expense of the smaller grains. The rate of increase with depth is not uniform. At Dome C and Vostok, grain-size remains fine in the upper few tens of cm (1 m at Dome C, 50 cm at Vostok), whereas grains are larger at or near the surface at itb4 and itb5. A simple age/depth relationship suggests that accumulation is lower at the latter sites. There is little increase in grain-size at itb4 and itb5 below 50 cm.

CONCLUSION

Size parameters automatically obtained from digital images of snow grains allowed comparisons between samples acquired by different people at different locations in Antarctica. Similar results were obtained with various acquisition techniques (classical photos or digital camera) that can be used during any scientific expedition with minimum equipment and facilities. One of the most difficult problems is the separation of snow grains, which is solved by choosing a size parameter based on the contour of the objects, the mean convex radius, and a robust image-analysis technique based on skeletization of the objects.

Data from 42 sites in Antarctica were analyzed. For radiative balance (albedo), only the surface grains must be considered, so no large variations due to grain-size are expected in those areas, except between Terra Nova Bay and Dome C. For metamorphism studies, the profiles obtained down to 2 m depth and even better down to 5 m at Dome C could be used with the available density profiles to validate and improve snow-metamorphism model results (Dang and others, 1997; Genthon and others, 2001).

The database which has been initiated will be increased in order to obtain a map of grain-size variations of the Antarctic ice sheet. This will improve understanding of the snow metamorphism in Antarctica in relation to climatic parameters.

ACKNOWLEDGEMENTS

This research was carried out within the framework of the European Community project Polar Snow (Contract ENV4-CT95-0076), the SPOT4/Vegetation Preparatory Pro-

https://doi.org/10.3189/172756502781831016 Published online by Cambridge University Press

gram (96/CNES/0394), a Project on Glaciology and Paleoclimatology of the Programma Nazionale di Ricerche in Antartide (PNRA), and was financially supported by Ente per le Nuove Tecnologie, l'Energia e l'Ambiente (ENEA) through a cooperation agreement with the Universit degli Studi di Milano. This work is a contribution of the Italian branch of the ITASE project. The authors wish to thank all members of the traverse teams, and the institutes which were in charge of the logistics: Institut Français de Recherche et Technologie Polaire (IFRTP), France; ENEA, Italy; Alfred Wegener Institute for Polar and Marine Research, Germany; Norwegian Polar Institute. A. Hubert (South Through the Pole Expedition) made a vital contribution to the design and tests of field photographic equipment.

REFERENCES

Alley, R. B. 1980. Densification and recrystallization of firn at Dome C, East Antarctica. *Ohio State Univ. Inst. Polar Stud. Rep.* 77.

Alley, R. B. 1987. Texture of polar firn for remote sensing. *Ann. Glaciol.*, **9**, 1–4.

Alley, R. B. and C. R. Bentley. 1988. Ice-core analysis on the Siple Coast of West Antarctica. *Ann. Glaciol.*, **11**, 1–7.

Arnaud, L., V. Lipenkov, J. M. Barnola, M. Gay and P. Duval. 1998. Modelling of the densification of polar firn: characterization of the snow–firn transition. *Ann. Glaciol.*, **26**, 39–44.

Bindschadler, R. 1998. Monitoring ice sheet behavior from space. *Rev. Geophys.*, **36**(1), 79–104.

Borgefors, G. 1986. Distance transformations in digital images. *Computer Vision, Graphics and Image Processing*, **34**(198), 344–371.

Brun, E. and E. Pahaut. 1991. An efficient method for a delayed and accurate characterization of snow grains from natural snowpacks. *J. Glaciol.*, **37**(127), 420–422.

Brun, E., E. Martin, V. Simon, C. Gendre and C. Coléou. 1989. An energy and mass model of snow cover suitable for operational avalanche forecasting. *J. Glaciol.*, **35**(121), 333–342.

Brun, E., P. David, M. Sudul and G. Brunot. 1992. A numerical model to simulate snow-cover stratigraphy for operational avalanche forecasting. *J. Glaciol.*, **38**(128), 13–22.

Chassery, J. M. and A. Montanvert. 1991. *Géométrie discrète en analyse d'images.* Paris, Edition Hermès.

Colbeck, S. C. 1991. The layered character of snow covers. *Rev. Geophys.*, **29**(1), 81–96.

Colbeck, S. C. *and 7 others*. 1990. *The international classification for seasonal snow on the ground.* Wallingford, Oxon, International Association of Scientific Hydrology. International Commission on Snow and Ice.

Dang, H., C. Genthon and E. Martin. 1997. Numerical modeling of snow cover over polar ice sheets. *Ann. Glaciol.*, **25**, 170–176.

Fily, M., B. Bourdelles, J.-P. Dedieu and C. Sergent. 1997. Comparison of in situ and Landsat thematic mapper derived snow grain characteristics in the Alps. *Remote Sensing Environ.*, **59**(3), 452–460.

Fily, M., C. Leroux, J. Lenoble and C. Sergent. 1998. Terrestrial snow studies from remote sensing in the Solar spectrum and the thermal infrared. *In* Schmitt, B., C. D. Bergh and M. Festou, *eds. Solar system ices.* Dordrecht, etc., Kluwer Academic Publishers, 421–441. (Astrophysics and Space Science Library 227.)

Fily, M., J. P. Dedieu and Y. Durand. 1999. Comparison between the results of a snow metamorphism model and remote sensing derived snow parameters in the Alps. *Remote Sensing Environ.*, **68**(3), 254–263.

Frezzotti, M., S. Gandolfi, F. La Marca and S. Urbini. 2002. Snow dunes and glazed surfaces in Antarctica: new field and remote-sensing data. *Ann. Glaciol.*, **34**, 81–88.

Genthon, C., M. Fily and E. Martin. 2001. Numerical simulations of Greenland snowpack and comparison with passive microwave spectral signatures. *Ann. Glaciol.*, **32**, 109–115.

Good, W. 1989. Laboratory techniques for the characterization of snow structure. *In* Hunt, J. and T. D. Guyenne, *eds. International Workshop on Physics and Mechanics of Cometary Materials, October 9–11, 1989, Münster, Westfalia, Germany. Proceedings*. Noordwijk, European Space Agency, 147–151. (ESA SP-302.)

Gow, A ,J. 1965. On the accumulation and seasonal stratification of snow at the South Pole. *J. Glaciol.*, **5**(40), 467–477.

Grenfell, T. C., S. G. Warren and P. C. Mullen. 1994. Reflection of solar radiation by the Antarctic snow surface at ultraviolet, visible, and near-infrared wavelengths. *J. Geophys. Res.*, **99**(D9), 18,669–18,684.

Lesaffre, B., E. Pougatch and E. Martin. 1998. Objective determination of snow-grain characteristics from images. *Ann. Glaciol.*, **26**, 112–118.

Marshall, S. and R. J. Oglesby. 1994. An improved snow hydrology for GCMs. Part 1: Snow cover fraction, albedo, grain size, and age. *Climate Dyn.*, **10**(1–2), 21–37.

Mayewski, P. A. and I. Goodwin. 1999. Antarctic's role pursued in global climate change. *Eos*, **80**(35), 398–400.

Sanniti di Baja, G. and E. Thiel. 1996. Skeletization algorithm running on path-based distance maps. *Image Vision Comput.*, **14**, 47–57.

Sergent, C., C. Leroux, E. Pougatch and F. Guirado. 1998. Hemispherical–directional reflectance measurements of natural snows in the 0.9–1.45 μm spectral range: comparison with adding–doubling modelling. *Ann. Glaciol.*, **26**, 59–63.

Stuart, A.W. and A. J. Heine. 1961. *Glaciology, Victoria Land traverse, 1959–60.* Columbus, OH, Ohio State University. Research Foundation. Institute of Polar Studies. (Report 968-1.)

Surdyk, S. and M. Fily. 1993. Comparison of the passive microwave spectral signature of the Antarctic ice sheet with ground traverse data. *Ann. Glaciol.*, **17**, 161–166.

Thiel, E. 1994. Les distances de chanfrein en analyse d'images: fondements et applications. (Ph.D. thesis, Université Joseph Fourier, Grenoble I.)

Wiesmann, A., C. Fierz and C. Mätzler. 2000. Simulation of microwave emission from physically modeled snowpacks. *Ann. Glaciol.*, **31**, 397–405.

Winther, J.-G. 1994. Spectral bi-directional reflectance of snow and glacier ice measured in Dronning Maud Land, Antarctica. *Ann. Glaciol.*, **20**, 1–5.

Winther, J.-G. *and 9 others*. 1997. EPICA Dronning Maud Land pre-site survey 1996/97. *In* Winther, J.-G., *ed. Report of the Norwegian Antarctic Research Expedition (NARE) 1996/97.* Oslo, Norsk Polarinstitutt, 96–117. (Meddelelser 148.)

MS received 10 August 2001 and accepted in revised form 15 August 2002